

Stabilization of high-temperature superconducting A15 phase La_4H_{23} below 100 GPa

Jianning Guo,^{1,†} Grigoriy Shutov,^{4,5,6,†} Su Chen,¹ Yulong Wang,¹ Di Zhou,³ Tian Cui^{1,2}, Xiaoli Huang,^{1,*} Dmitrii Semenok,^{3,*}

¹*State Key Laboratory of Superhard Materials, College of Physics, Jilin University, Changchun 130012, China*

²*School of Physical Science and Technology, Ningbo University, Ningbo 315211, China*

³*Center for High Pressure Science and Technology Advanced Research (HPSTAR), Beijing*

⁴ *Moscow Institute of Physics and Technology, 9 Institutsky Lane, Dolgoprudny 141700, Russia*

⁵ *Dukhov Research Institute of Automatics (VNIIA), Moscow 127055, Russia*

⁶ *Skolkovo Institute of Science and Technology, Skolkovo Innovation Center, 3 Nobel Street, Moscow 143026, Russia*

[†]These authors contributed equally to this work

*Corresponding authors, Email: huangxiaoli@jlu.edu.cn (X. Huang)
dmitrii.semenok@hpstar.ac.cn (D. Semenok)

Abstract

High pressure plays a crucial role in the field of superconductivity. Compressed hydride superconductors are leaders in the race for a material that can conduct electricity without resistance at high or even room temperature. Different synthetic paths under pressure will drive the formation of different polyhydrides. In the present work, through precise control of the synthesis pathways, we have discovered new lanthanum superhydride, cubic A15-type La_4H_{23} , with lower stabilization pressure compared to the reported *fcc* LaH_{10} . Superconducting La_4H_{23} was obtained by laser heating of LaH_3 with ammonia borane at about 120 GPa. Transport measurements reveal the maximum critical temperature $T_C(\text{onset}) = 105$ K at 118 GPa, as evidenced by the sharp drop of electrical resistance and the displacement of superconducting transitions in applied magnetic fields. Extrapolated upper critical field $B_{C2}(0)$ of La_4H_{23} is about 33 T at 114 GPa in agreement with theoretical estimates. Discovered lanthanum hydride is a new member of the A15 family of superconductors with T_C exceeding the boiling point of liquid nitrogen.

Introduction

The search for high-temperature superconductivity has been an important goal pursued tirelessly by researchers since the discovery of the superconductivity in mercury [1]. However, until 1986, the critical temperature of conventional superconductors had never exceeded the McMillan limit (30-40 K) [2]. As one of the most effective methods of changing the structure of matter, pressure can lead to appearance of unusual properties of matter that are unlikely to occur in normal conditions, such as high-temperature superconductivity (HTSC). The increase of the critical temperature of superconductivity in cuprates under pressure to 164 K motivated extensive research in the high pressure field [3]. On the basis of the chemical pre-compression idea, first proposed by Ashcroft [4], the breakthrough discovery of HTSC in compressed sulfur hydride H_3S with T_C above 200 K at 150 GPa was made both theoretically and experimentally in 2014-2015 [5, 6]. Soon after, the HTSC record was broken by lanthanum superhydride LaH_{10} with $T_C = 250$ K at 170 GPa [7, 8]. The successful use of high pressure in the search for new superconductors provided a clear path to even room-temperature superconductivity and attracted considerable scientific interest. Over the past five years, such remarkable

superconductors as YH_6 [9], YH_9 [10], CeH_{10} [11] and CaH_6 [12] have been found.

In addition to the experimental results, there are a number of theoretically predicted high-temperature superconducting hydrides, such as YH_{10} [13], HfH_{10} [14] and $\text{Li}_2\text{MgH}_{16}$ [15]. However, many of them are metastable and cannot be obtained under real experimental conditions. The high temperature and high pressure environment is considered to be essential for experimental synthesis of superhydrides to overcome kinetic barriers. [16]. Different reaction conditions, amounts of hydrogen, and pathways will lead to different mixtures of resulting polyhydrides so that we can intercept the desired compounds at target pressures and temperatures. To date, LaH_{10} has the highest T_C among binary hydrides, and the La-H system is one of the best studied both experimentally and theoretically [13, 17-24]. Recently, a series of novel lanthanum hydrides was found using single-crystal X-ray diffraction analysis including traces of $Pm\bar{3}n$ - La_4H_{23} [21]. However, due to the complex composition of the mixture and the low content of this phase, the transport properties of La_4H_{23} have not been studied.

$\text{A}15$ (β -W) structural type is a series of intermetallic compounds with outstanding low-temperature superconducting properties and $Pm\bar{3}n$ symmetry. Examples are vanadium silicide V_3Si ($T_C = 17$ K), Nb_3Ge ($T_C = 23.2$ K) and Nb_3Sn ($T_C = 18.3$ K). In this work, we have successfully synthesized a new representative of this class, cubic La_4H_{23} with $\text{A}15$ structure, stable in the pressure range of 91–120 GPa, using laser heating of LaH_3 with ammonia borane (NH_3BH_3) above 2000 K. Transport measurements showed a sharp drop of the sample electrical resistance in 10^3 times with the highest onset $T_C = 105$ K, and the decrease of the critical temperature under external magnetic fields. Theoretical calculations support conclusions of the experiment and point to a strong electron-phonon interaction in the hydrogen sublattice of $Pm\bar{3}n$ - La_4H_{23} .

Experimental details

In this work, we used powder LaH_{3-x} ($x \approx 0.1$ –0.2) with metallic conductivity, which was preliminarily synthesized from La powder and hydrogen, and ammonia borane (AB, NH_3BH_3) as the hydrogen source and pressure transmitting medium, considering the high-temperature decomposition reaction: $\text{NH}_3\text{BH}_3 \rightarrow 3\text{H}_2 + \text{c-BN}$ [11]. All the crystal structures were determined by *in situ* high-pressure X-ray diffraction (XRD) at the SPring-8 (Japan) synchrotron radiation source, beamline BL10XU, using the wavelength of 0.4124 Å. The CeO_2 was used as a calibrant. Dioptas software was used to analyze the experimental XRD patterns [25].

Diamond anvil cells (DACs) are essential for high-pressure experiments, and we used the DACs made of NiCrAl alloy. Diamond anvils had a culet of 60 µm, beveled at 8° to a diameter of 250 µm. For transport measurements, the MgO/epoxy was selected as insulting layer placed between the tungsten gasket and platinum leads. Molybdenum electrodes were sputtered on the surface of diamond anvils to connect the sample and Pt leads. The pressure was determined by the diamond Raman shift [26]. Further experimental details described in the Supporting Information.

Computational details

The evolutionary algorithm USPEX [27-29] was used to predict thermodynamically stable La-H phases. To investigate the La-H system, we performed both fixed- and variable-composition searches at 100, 120, 150 and 200 GPa. The number of generations was 100. We calculated the convex hulls in the temperature range from 0 K to 2000 K, using free energies computed by Phonopy [30]. Metastable structures with the energy ≤ 30 meV/atom above the hull are also presented on the convex hulls.

Structure relaxations and energy calculations were performed using the VASP code[31-33] within density

functional theory (DFT)[34, 35], implementing the Perdew–Burke–Ernzerhof (PBE) exchange–correlation functional[36] and the projector-augmented wave (PAW) method[37, 38]. The kinetic energy cutoff was set at 600 eV. Γ -centered k-point meshes with a resolution of $2\pi \times 0.05 \text{ \AA}^{-1}$ were used for sampling the Brillouin zone. The phonon band structure and density of states were computed using Phonopy [30] package implementing the finite displacement method, $2 \times 2 \times 2$ supercells were generated. The energy cutoff and k-spacing parameters for the VASP calculations were set at 500 eV and $2\pi \times 0.1 \text{ \AA}^{-1}$, respectively. Sumo package [39] was used to visualize the phonon density of states and band structure. The k-points for phonon band structures were chosen using Hinuma’s recommendation [40]. The Phonopy package was also used to calculate zero-point energy (ZPE) corrections and thermal properties, such as entropy and free energy. To calculate phonon frequencies and electron–phonon coupling (EPC) coefficients, we used Quantum Espresso (QE) package [41] utilizing density functional perturbation theory (DFPT) [42], plane-wave PZ HGH pseudopotentials and the tetrahedron method [43, 44].

Results and discussions

Superconducting properties of La₄H₂₃

In this work, the NH₃BH₃ was loaded into the chamber as the hydrogen source and pressure transmitting medium [11]. The scheme of the electrical DAC H1 prepared for the transport measurements is shown in Figures 1a, b. Laser heating of the LaH₃/AB sample to temperature above 2000 K was performed at 123 GPa, then the pressure reduced to 120 GPa. Cryogenic measurements of the sample immediately showed the appearance of a drop in electrical resistance from 0.12 Ohm to 10^{-4} Ohm at 93 K corresponding to the manifestation of superconductivity in the sample. After the second laser heating, a sharp superconducting transition was observed at 90 K at 114 GPa. The third laser heating led to an increase in pressure to 118 GPa and the critical temperature T_c also rose to 105 K. This value is very close to the critical temperatures of cerium superhydrides CeH₉ and CeH₁₀ in the same pressure range [11], but the advantage of the studied La₄H₂₃ is the much smaller amount of hydrogen required to obtain this result. To further investigate the dependence of T_c on pressure, we decompressed the DAC to 91 GPa (Figure 1c). We found that $T_c(P)$ decreases monotonically during the decompression reaching the maximum of 105 K at 118 GPa (Figure 1d).

Remarkably, a change in the sign of the quasi-linear temperature dependence of the electrical resistance (dR/dT) is observed during decompression (Figure 1c) of the DAC H1. This phenomenon was previously observed during decompression in sulfur hydrides H₂S and H₃S [6], in phosphorus hydride PH₃ [45], in CeH₁₀ [46] and in ternary superhydride (La,Ce)H₉ [47]. As we have shown earlier for SnH₄ [48], the change in the sign of dR/dT is incompatible with the view of La₄H₂₃ as a normal Fermi-liquid metal whose resistance is due to the scattering of electrons on phonons. Instead, the properties of polyhydrides in the non-superconducting state on the verge of their dynamic stability [49] should be described in the framework of a non-Fermi liquid model close to the models developed for describing the pseudogap phase and metal-to-insulator transitions in cuprates [50]. In general, decompression of DAC H1 leads to broadening of superconducting transitions up to complete disappearance of the superconducting state and decomposition of La₄H₂₃ (Figures 1c, d).

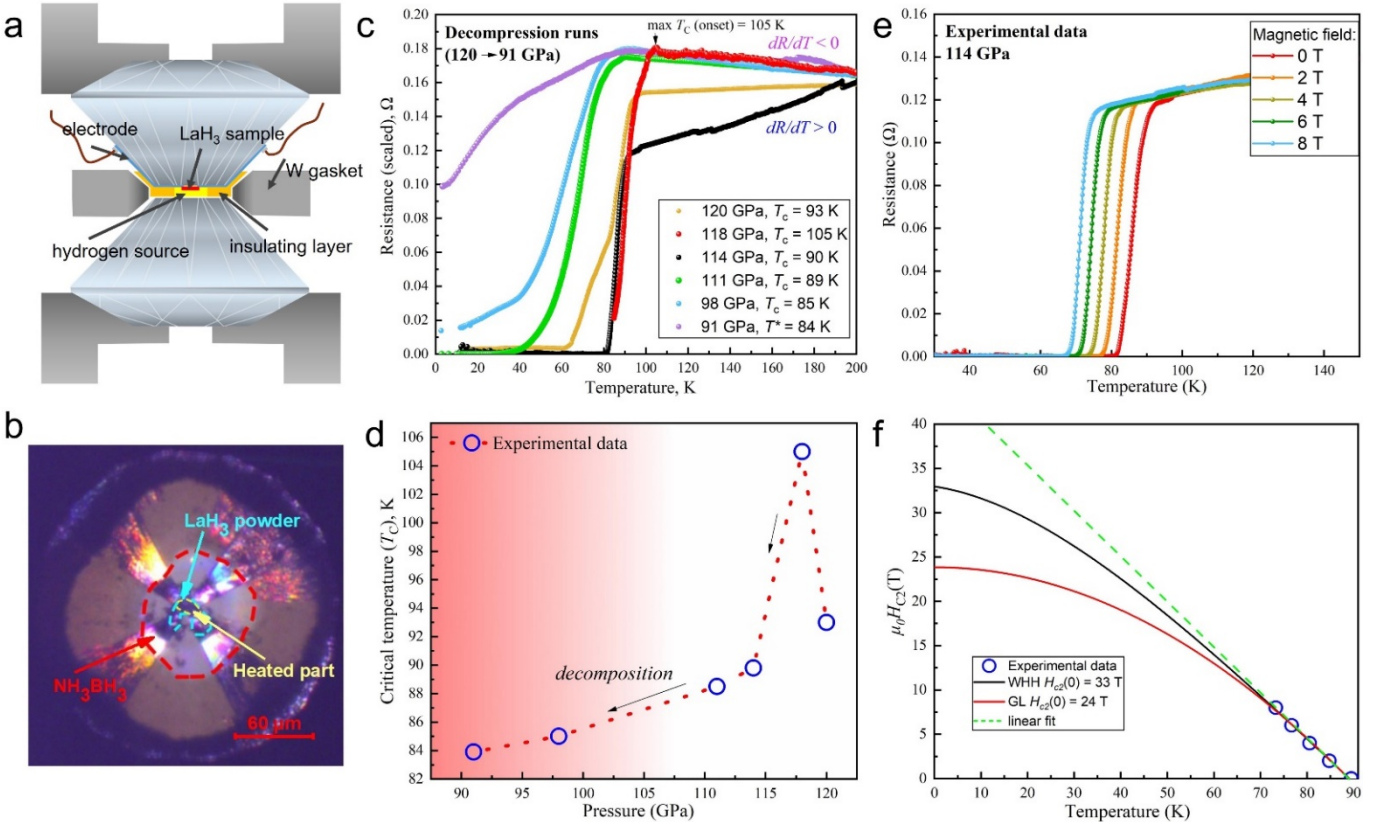


Figure 1. Electrical DAC construction and transport properties of La_4H_{23} under pressure. (a) Schematic diagram of the electrical DAC with the four-electrode van der Pauw scheme. (b) Photograph of the sample loaded in the DAC's chamber and four Mo electrodes after the laser heating at 114 GPa. The hydrogen source (NH_3BH_3) and the LaH_3 are indicated by red and blue curves, respectively. (c) Dependence of the electrical resistance of the sample on temperature during decompression of DAC H1 from 120 GPa to 91 GPa. T_c corresponds to the onset transition point. (d) Pressure dependence of the critical temperature of La_4H_{23} . (e) Dependence of electrical resistance of the sample on applied magnetic field at 114 GPa. (f) Magnetic phase diagram $B_{c2}(T)$ of La_4H_{23} at 114 GPa obtained by extrapolation of the experimental data using the Ginzburg-Landau (GL), [51] the Werthamer-Helfand-Hohenberg (WHH) [52, 53] and linear models.

To further confirm the superconductivity, we measured the electrical resistance of the sample in DAC H1 in magnetic fields ranging from 0 to 8 T. Figure 1e shows the temperature dependence of electrical resistance of La_4H_{23} in applied fields at 114 GPa. The sample demonstrates the absence (or even negative value) of broadening of superconducting transitions in a magnetic field, as previously observed for yttrium (YH_6) [54] and lanthanum-yttrium ($(\text{La},\text{Y})\text{H}_{10}$) hydrides [55]. T_c shifts linearly to lower temperatures as the magnetic field increases from 0 to 8 T, as it should for superconductors. To estimate the upper critical magnetic field $B_{c2}(0)$, we applied the GL model [51], and the WHH model [52], simplified by Baumgartner [53]. As Figure 1f shows, these two models yield the $B_{c2}(0)$ as 24 T and 33 T, respectively. The coherence length can be estimated by $\mu_0 H_{c2} = \Phi_0 / (2\pi\zeta^2)$ [56]. The $\zeta_{WHH}(0)$ and $\zeta_{GL}(0)$ are equal to 3.16 nm and 3.72 nm, respectively. These values are higher than the same parameters in *fcc* LaH_{10} [56].

Interestingly, the superconducting properties of La_4H_{23} are found to be more pronounced than those of the recently studied A15 Lu_4H_{23} (max $T_c = 71$ K, [57]). This indicates that isostructural lutetium compounds, such as proposed LuH_{10} , LuH_9 , and LuH_6 , will have lower critical temperatures than the corresponding lanthanum polyhydrides in contradiction with earlier theoretical predictions [58]. Moreover, due to the smaller atomic radius

of Lu, we would have to apply much higher pressures to stabilize the corresponding lutetium hydrides (e.g., LuH_{10}), making them less convenient to study than LaH_x .

Crystal structure of La_4H_{23}

For the first time among polyhydrides, structural type A15 ($Pm\bar{3}n$) was found when studying the formation of europium hydrides [59] above 100 GPa. Then, polyhydrides with the same structure were found in Ba-H system [60], among lanthanum [21] and lutetium [57] polyhydrides. As we found out in the previous section, La_4H_{23} has the highest T_C among all superconductors with A15 structure. Below we discuss the results of X-ray diffraction analysis of this compound.

Considering the large number of superconducting phases in the La-H system at megabar pressures, we have combined the experimental XRD data and the computational crystal structure search to determine the crystal structures [21]. In Figure 2a, the in-situ synchrotron X-ray diffraction patterns indicate that the DAC H1 sample possessing $Pm\bar{3}n$ symmetry at 118 GPa. The volume of the unit cell is $28.9 \text{ \AA}^3/\text{La}$ and $a = 6.14 \text{ \AA}$ ($Z = 8$), which is in close agreement with the theoretical results in 118 GPa ($\approx 28 \text{ \AA}^3/\text{La}$, see Supporting Figure S9). We also compared obtained unit cell volume of $Pm\bar{3}n$ - La_4H_{23} with the reported one [21], which is $27.98 \text{ \AA}^3/\text{La}$ at 150 GPa. This is slightly different due to higher pressure in the Laniel et al. experiment. The hydrogen content can be estimated by the difference between atomic volumes of La atoms and the hydrogen [61, 62].

Figure 2b shows a series of XRD patterns measured at several positions across the sample in steps of $5 \mu\text{m}$. All XRD images are almost identical at all locations containing the signals from the Mo electrodes and $Pm\bar{3}n$ - La_4H_{23} . This confirms the uniform distribution of hydrogen and selective formation of only one phase in the process of synthesis. In the hydrogen cage of La_4H_{23} , the shortest H-H distance is about 1.3 \AA at 118 GPa, which is in the range of $1.0 - 1.5 \text{ \AA}$ for typical hydride superconductors. This bond length is much longer than in pure $\text{H}_2 \sim 1.1 \text{ \AA}$ at 115 GPa [22].

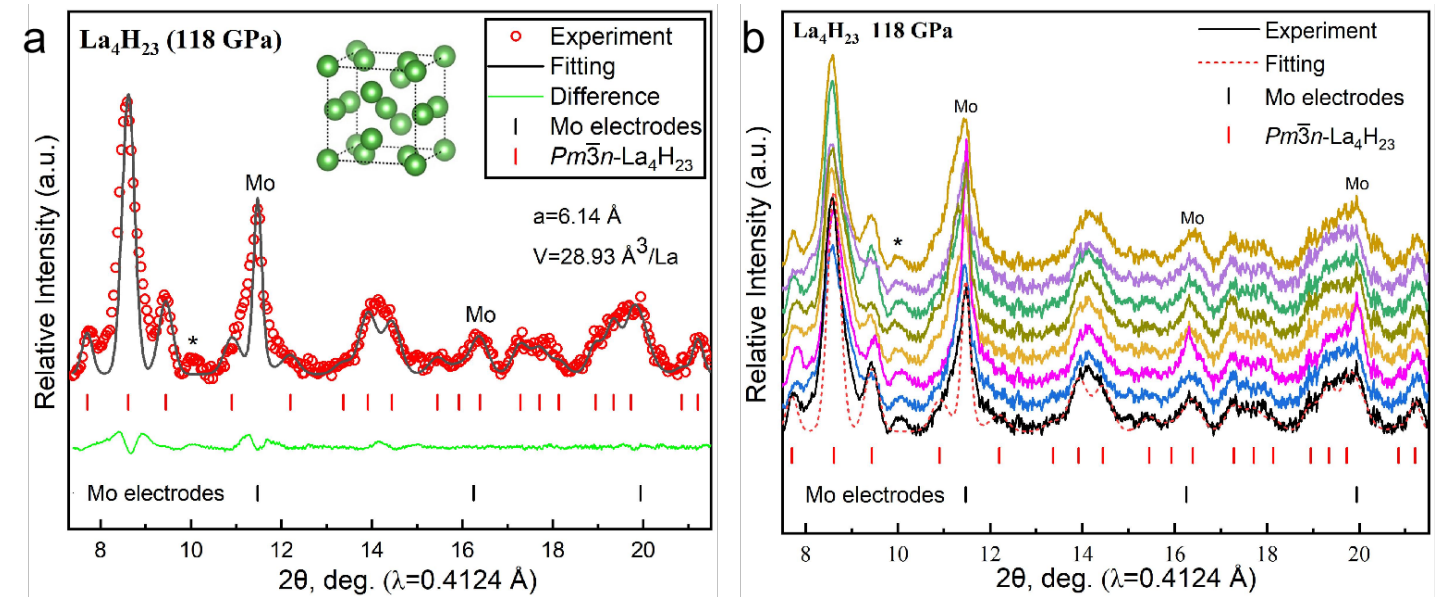


Figure 2. X-ray diffraction and crystal structure of La_4H_{23} . (a) X-ray diffraction pattern and Le Bail refinement of the unit cell parameters of La_4H_{23} phase at 118 GPa. Experimental XRD data and the Le Bail fit are represented by red hollow circles and black lines, respectively. XRD pattern contains spurious signals from molybdenum (Mo) electrodes. (b) XRD patterns measured across the sample with a step of $5 \mu\text{m}$.

Theoretical analysis

We have performed a series of thermodynamic calculations of the enthalpies of formation of various lanthanum polyhydrides at 100, 120, 150, and 200 GPa and temperatures from 0 to 2000 K, considering the zero-point energy (ZPE) contribution in the harmonic approximation. The corresponding convex hulls are shown in Supporting Figures S1-S6. As can be seen, $Pm\bar{3}n$ -La₄H₂₃ is close to the stability region and about 20-30 meV/atom above the convex hull at 100-150 GPa. This phase is dynamically stable at 120 GPa already in the harmonic approximation (Figure 3b), although further pressure reduction to 100 GPa destabilizes it. Increasing the temperature has little effect on its relative stability (Supporting Figures S4-S6), whereas the stability of the nearby highly symmetric phases $Im\bar{3}m$ -LaH₆ and $Fm\bar{3}m$ -LaH₁₀ is strongly affected. We find that $Im\bar{3}m$ -LaH₆ is dynamically unstable in the harmonic approximation at 100-120 GPa and can undergo distortion $Im\bar{3}m \rightarrow Cmme \rightarrow C2/m$ at low pressure, which stabilizes La₄H₂₃. This is also supported by the known experimental fact of LaH₁₀ distortion at pressures below 140 GPa [20]. Thus, the convex hull deformation at low pressures caused by a much faster destabilization of the $Im\bar{3}m$ -LaH₆ structure may lead to the possibility of experimentally obtaining $Pm\bar{3}n$ -La₄H₂₃. Indeed, all lanthanum hydrides discussed above were synthesized in recent experiments [21].

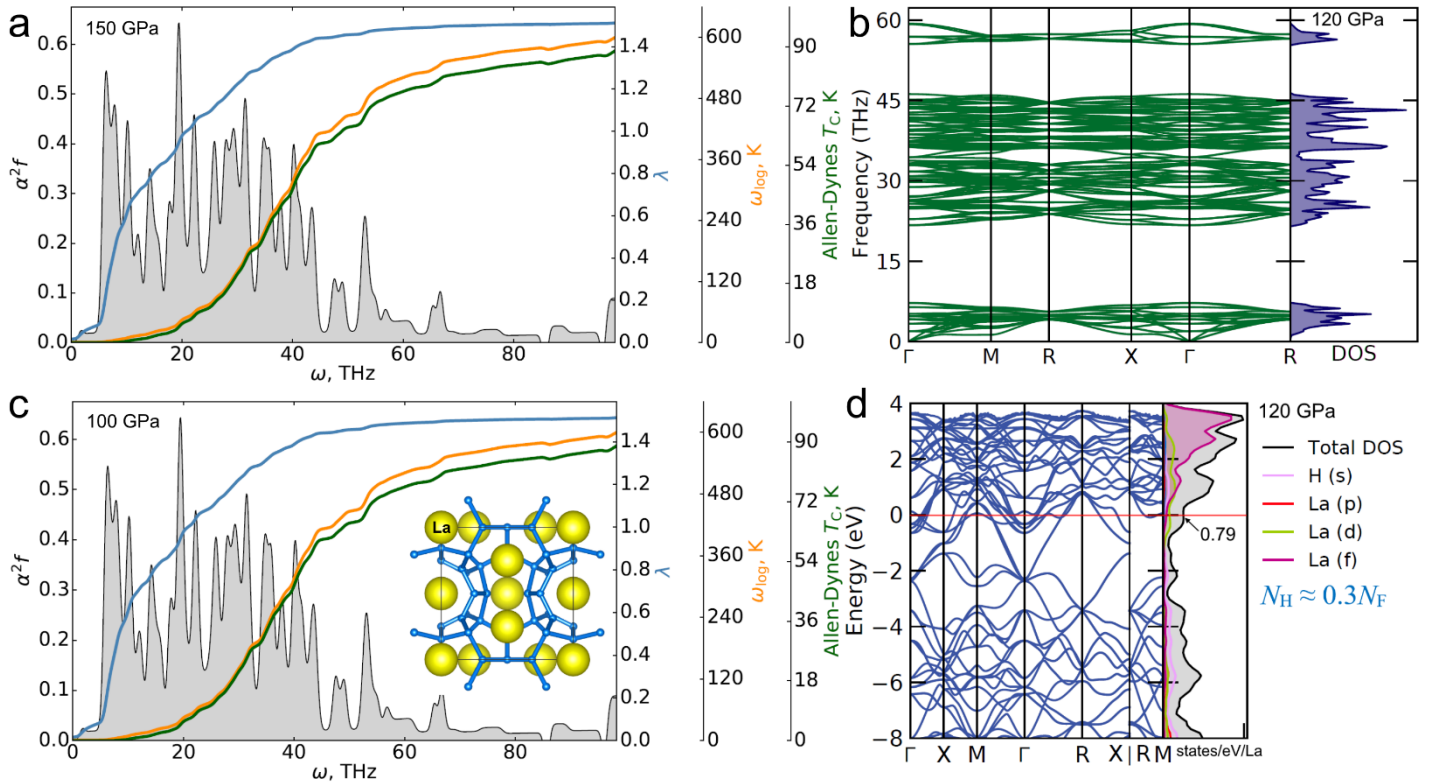


Figure 3. Results of theoretical calculations of electronic, phonon and superconducting properties of La₄H₂₃ at 100, 120 and 150 GPa. (a, c) Eliashberg functions of La₄H₂₃ calculated at 150 and 100 GPa, respectively. We used a k-mesh of 8×8×8 and a q-mesh of 2×2×2. The results were also verified on k-mesh 12×12×12 and q-mesh 3×3×3. (b) Phonon band structure and density of states of La₄H₂₃ at 120 GPa calculated in the harmonic approximation. The compound was found to be dynamically stable at this pressure. (d) Electron band structure and density of states projected on H and La atoms at 120 GPa. The contribution of hydrogen is ≈ 30 % of the total density of states.

Superconducting properties of $Pm\bar{3}n$ -La₄H₂₃ have been investigated theoretically using the norm-conserving Goedecker-Hartwigsen-Hutter (GHH) pseudopotential with the Perdew-Zunger (LDA) functional and k , q -grids of low density. These pseudopotentials give results that are in good agreement with the experimental

data, so it is this computational approach that we will discuss in the following (Table 1 and Figure 3 a, c). We find that La_4H_{23} exhibits moderate superconducting properties at 100 GPa, where electron-phonon interaction strength $\lambda \approx 1.5$, which decreases with increasing pressure due to a decrease in the λ . The calculated critical temperature of superconductivity (T_c) of La_4H_{23} reaches 92-95 K at 100 GPa in the harmonic approximation. The relatively low T_c of this superhydride correlates with the low contribution of the hydrogen sublattice to the density of electronic states (Figure 3d), which is equal to about 30% of the total density of electronic states at the Fermi level (N_F). The expected [63] upper critical magnetic field $\mu_0 H_{c2}(0) = 51$ T is accessible for modern pulsed magnets.

Table 1. Parameters of the superconducting state of $Pm\bar{3}n$ - La_4H_{23} calculated at 100 and 150 GPa in the harmonic approximation using HGH PZ pseudopotentials. “McM” stands for the McMillan formula [2], “A-D” stands for the Allen-Dynes model [64], and “E” corresponds to the solution of the isotropic Eliashberg equations [65] ($\mu^* = 0.1$ in all cases).

| Pressure | 100 GPa | 150 GPa |
|---------------------------------------|---------|---------|
| λ | 1.49 | 1.0 |
| ω_{log} , K | 650 | 892 |
| ω_2 , K | 1121 | 1383 |
| T_c (McM) | 73.5 | 61.4 |
| T_c (A-D) | 91.7 | 68.0 |
| T_c (E) | 94.7 | 70.4 |
| N_F , states/spin/Ry/Å ³ | 0.196 | 0.182 |
| $2\Delta/k_B T_c$ | 4.69 | 4.04 |
| Expected $B_{c2}(0)$, T* | 51 | 29 |
| 2Δ , meV | 19.1 | 12.2 |

Conclusions

We have synthesized novel lanthanum superhydride La_4H_{23} with the A15 structure via laser heating of LaH_3 and NH_3BH_3 at 118-123 GPa. X-ray diffraction revealed a $Pm\bar{3}n$ - La_4H_{23} phase as the main reaction product, which has a clathrate hydrogen sublattice. Transport measurements confirm pronounced superconducting properties of La_4H_{23} with a maximum superconducting transition temperature of 105 K at 118 GPa in agreement with theoretical calculations. During decompression, T_c of La_4H_{23} decreases along with the pressure below 118 GPa, and at 91 GPa the superconducting transition completely disappears. In the non-superconducting state between 98 and 120 GPa, La_4H_{23} demonstrates a change in the sign of the quasi-linear temperature dependence of the electrical resistance corresponding to the non-Fermi liquid (strange metal) behavior. The extrapolated upper critical magnetic field $B_{c2}(0)$ is estimated to be 33 T, the coherence length $\zeta_{W\text{HH}}(0)$ is 3.16 nm, and the calculated electron-phonon interaction strength λ is around 1.5.

Author statement

Jianning Guo: Validation, formal analysis, investigation, visualization, writing-original draft. **Grigoriy Shutov:** Validation, theoretical analysis, investigation, visualization. **Su Chen:** Investigation. **Yulong Wang:**

Investigation. **Di Zhou**: Investigation. **Tian Cui**: Writing and review & editing, funding acquisition. **Xiaoli Huang**: Investigation, writing-review & editing, funding acquisition. **Dmitrii Semenok**: Investigation, writing original draft, theoretical calculations, review & editing.

Declaration of competing interest

The authors declare no competing financial interest or personal relationships that could have appeared to influence the work reported in this paper.

Data availability

The authors declare that the main data supporting the findings of this study are contained within the paper and its associated Supporting Information. All other relevant data are available from the corresponding author upon reasonable request.

Acknowledgements

Authors thank the staff of SPring-8 Synchrotron Radiation Facility for their help during the synchrotron XRD measurements.

Funding

This work was supported by National Key R&D Program of China (2022YFA1405500), the National Natural Science Foundation of China (11974133 and 52072188), the Program for Changjiang Scholars and Innovative Research Team in University (IRT_15R23), and users with Excellence Program of Hefei Science Center CAS 2021HSC-UE011, Zhejiang Provincial Science and technology innovation Team (2021R01004), and Jilin Provincial Science and Technology Development Project (20210509038RQ), the Fundamental Research Funds for the Central Universities.

References

- [1] H.K. Onnes, The superconductivity of mercury., Comm Phys Lab Univ Leiden, (1911) 122-124.
- [2] W.L. McMillan, Transition Temperature of Strong-Coupled Superconductors, Physical Review, 167 (1968) 331-344.
- [3] L. Gao, Y.Y. Xue, F. Chen, Q. Xiong, R.L. Meng, D. Ramirez, C.W. Chu, J.H. Eggert, H.K. Mao, Superconductivity up to 164 K in $HgBa_2Cam-1CumO_{2m+2+\delta}$ ($m=1, 2$, and 3) under quasihydrostatic pressures, Phys Rev B Condens Matter, 50 (1994) 4260-4263.
- [4] N.W. Ashcroft, Hydrogen dominant metallic alloys: high temperature superconductors?, Phys Rev Lett, 92 (2004) 187002.
- [5] D. Duan, Y. Liu, F. Tian, D. Li, X. Huang, Z. Zhao, H. Yu, B. Liu, W. Tian, T. Cui, Pressure-induced metallization of dense $(H_2S)_2H_2$ with high-Tc superconductivity, Sci Rep, 4 (2014) 6968.
- [6] A.P. Drozdov, M.I. Eremets, I.A. Troyan, V. Ksenofontov, S.I. Shylin, Conventional superconductivity at 203 kelvin at high pressures in the sulfur hydride system, Nature, 525 (2015) 73-76.
- [7] M. Somayazulu, M. Ahart, A.K. Mishra, Z.M. Geballe, M. Baldini, Y. Meng, V.V. Struzhkin, R.J. Hemley, Evidence for Superconductivity above 260 K in Lanthanum Superhydride at Megabar Pressures, Phys Rev Lett,

122 (2019) 027001.

- [8] A.P. Drozdov, P.P. Kong, V.S. Minkov, S.P. Besedin, M.A. Kuzovnikov, S. Mozaffari, L. Balicas, F.F. Balakirev, D.E. Graf, V.B. Prakapenka, E. Greenberg, D.A. Knyazev, M. Tkacz, M.I. Eremets, Superconductivity at 250 K in lanthanum hydride under high pressures, *Nature*, 569 (2019) 528-531.
- [9] I.A. Troyan, D.V. Semenok, A.G. Kvashnin, A.V. Sadakov, O.A. Sobolevskiy, V.M. Pudalov, A.G. Ivanova, V.B. Prakapenka, E. Greenberg, A.G. Gavriliuk, I.S. Lyubutin, V.V. Struzhkin, A. Bergara, I. Errea, R. Bianco, M. Calandra, F. Mauri, L. Monacelli, R. Akashi, A.R. Oganov, Anomalous High-Temperature Superconductivity in YH₆, *Adv Mater*, 33 (2021) e2006832.
- [10] P. Kong, V.S. Minkov, M.A. Kuzovnikov, A.P. Drozdov, S.P. Besedin, S. Mozaffari, L. Balicas, F.F. Balakirev, V.B. Prakapenka, S. Chariton, D.A. Knyazev, E. Greenberg, M.I. Eremets, Superconductivity up to 243 K in the yttrium-hydrogen system under high pressure, *Nat Commun*, 12 (2021) 5075.
- [11] W. Chen, D.V. Semenok, X. Huang, H. Shu, X. Li, D. Duan, T. Cui, A.R. Oganov, High-Temperature Superconducting Phases in Cerium Superhydride with a T_c up to 115 K below a Pressure of 1 Megabar, *Phys Rev Lett*, 127 (2021) 117001.
- [12] L. Ma, K. Wang, Y. Xie, X. Yang, Y. Wang, M. Zhou, H. Liu, X. Yu, Y. Zhao, H. Wang, G. Liu, Y. Ma, High-Temperature Superconducting Phase in Clathrate Calcium Hydride CaH₆ up to 215 K at a Pressure of 172 GPa, *Physical Review Letters*, 128 (2022).
- [13] H. Liu, Naumov, II, R. Hoffmann, N.W. Ashcroft, R.J. Hemley, Potential high-T_c superconducting lanthanum and yttrium hydrides at high pressure, *Proc Natl Acad Sci U S A*, 114 (2017) 6990-6995.
- [14] H. Xie, Y. Yao, X. Feng, D. Duan, H. Song, Z. Zhang, S. Jiang, S.A.T. Redfern, V.Z. Kresin, C.J. Pickard, T. Cui, Hydrogen Pentagraphenelike Structure Stabilized by Hafnium: A High-Temperature Conventional Superconductor, *Phys Rev Lett*, 125 (2020) 217001.
- [15] Y. Sun, J. Lv, Y. Xie, H. Liu, Y. Ma, Route to a Superconducting Phase above Room Temperature in Electron-Doped Hydride Compounds under High Pressure, *Phys Rev Lett*, 123 (2019) 097001.
- [16] X. Zhang, Y. Zhao, F. Li, G. Yang, Pressure-induced hydride superconductors above 200 K, *Matter and Radiation at Extremes*, 6 (2021).
- [17] M. Somayazulu, M. Ahart, A.K. Mishra, Z.M. Geballe, Evidence for Superconductivity above 260 K in Lanthanum Superhydride at Megabar Pressures, *PHYSICAL REVIEW LETTERS*, (2019) 027001.
- [18] A.P. Drozdov, V.S. Minkov, S.P. Besedin, P.P. Kong, Superconductivity at 215 K in lanthanum hydride at high pressures, *arxiv*, (2018) 07039.
- [19] F. Hong, L. Yang, P. Shan, P. Yang, Z. Liu, J. Sun, Y. Yin, X. Yu, J. Cheng, Z. Zhao, Superconductivity of Lanthanum Superhydride Investigated Using the Standard Four-Probe Configuration under High Pressures*, *Chinese Physics Letters*, 37 (2020).
- [20] D. Sun, V.S. Minkov, S. Mozaffari, Y. Sun, Y. Ma, S. Chariton, V.B. Prakapenka, M.I. Eremets, L. Balicas, F.F. Balakirev, High-temperature superconductivity on the verge of a structural instability in lanthanum superhydride, *Nat Commun*, 12 (2021) 6863.
- [21] D. Laniel, F. Trybel, B. Winkler, F. Knoop, T. Fedotenko, S. Khandarkhaeva, A. Aslandukova, T. Meier, S. Chariton, K. Glazyrin, V. Milman, V. Prakapenka, I.A. Abrikosov, L. Dubrovinsky, N. Dubrovinskaia, High-pressure synthesis of seven lanthanum hydrides with a significant variability of hydrogen content, *Nat Commun*, 13 (2022) 6987.
- [22] Z.M. Geballe, H. Liu, A.K. Mishra, M. Ahart, M. Somayazulu, Y. Meng, M. Baldini, R.J. Hemley, Synthesis

and Stability of Lanthanum Superhydrides, *Angew Chem Int Ed Engl*, 57 (2018) 688-692.

[23] I.A. Kruglov, D.V. Semenok, H. Song, R. Szczęśniak, I.A. Wrona, R. Akashi, M.M. Davari Esfahani, D. Duan, T. Cui, A.G. Kvashnin, A.R. Oganov, Superconductivity of LaH₁₀ and LaH₁₆ polyhydrides, *Physical Review B*, 101 (2020).

[24] M. Sakata, M. Einaga, M. Dezhong, T. Sato, S.-i. Orimo, K. Shimizu, Superconductivity of lanthanum hydride synthesized using AlH₃ as a hydrogen source, *Superconductor Science and Technology*, 33 (2020).

[25] C. Prescher, V.B. Prakapenka, DIOPTAS: a program for reduction of two-dimensional X-ray diffraction data and data exploration, *High Pressure Research*, 35 (2015) 223-230.

[26] Y. Akahama, H. Kawamura, Pressure calibration of diamond anvil Raman gauge to 310GPa, *Journal of Applied Physics*, 100 (2006).

[27] A.R. Oganov, C.W. Glass, Crystal structure prediction using ab initio evolutionary techniques: principles and applications, *J Chem Phys*, 124 (2006) 244704.

[28] A.R. Oganov, A.O. Lyakhov, M. Valle, How evolutionary crystal structure prediction works-and why, *Accounts of Chemical Research*, 44 (2011).

[29] A.O. Lyakhov, A.R. Oganov, H.T. Stokes, Q. Zhu, New developments in evolutionary structure prediction algorithm USPEX, *Computer Physics Communications*, 184 (2013) 1172-1182.

[30] A. Togo, I. Tanaka, First principles phonon calculations in materials science, *Scripta Materialia*, 108 (2015) 1-5.

[31] G. Kresse, J. Hafner, Ab initio molecular-dynamics simulation of the liquid-metal-amorphous-semiconductor transition in germanium, *Phys Rev B Condens Matter*, 49 (1994) 14251-14269.

[32] G. Kresse, Ab initio molecular dynamics for liquid metals, *Journal of Non-Crystalline Solids*, 222 (1995) 192-193.

[33] G. Kresse, Furthmuller, J., Efficient iterative schemes for ab initio total-energy calculations using a plane-wave basis set, *Phys. Rev. B*, 54, 11169 (1996).

[34] P. Hohenberg, W. Kohn, Inhomogeneous Electron Gas, *Physical Review*, 136 (1964) B864-B871.

[35] W. Kohn, L.J. Sham, Self-Consistent Equations Including Exchange and Correlation Effects, *Physical Review*, 140 (1965) A1133-A1138.

[36] J.P. Perdew, K. Burke, M. Ernzerhof, Generalized gradient approximation made simple, *Phys. Rev. Lett.*, 77, 3865 (1996).

[37] P.E. Blochl, Projector augmented-wave method, *Phys Rev B Condens Matter*, 50 (1994) 17953-17979.

[38] G. Kresse, D. Joubert, From ultrasoft pseudopotentials to the projector augmented-wave method, *Phys. Rev. B*, 59, 1758 (1999).

[39] A. M Ganose, A. J Jackson, D. O Scanlon, sumo: Command-line tools for plotting and analysis of periodic ab initio calculations, *Journal of Open Source Software*, 3 (2018).

[40] Y. Hinuma, G. Pizzi, Y. Kumagai, F. Oba, I. Tanaka, Band structure diagram paths based on crystallography, *Computational Materials Science*, 128 (2017) 140-184.

[41] P. Giannozzi, S. Baroni, N. Bonini, M. Calandra, R. Car, C. Cavazzoni, D. Ceresoli, G.L. Chiarotti, M. Cococcioni, I. Dabo, A. Dal Corso, S. de Gironcoli, S. Fabris, G. Fratesi, R. Gebauer, U. Gerstmann, C. Gougaud, A. Kokalj, M. Lazzeri, L. Martin-Samos, N. Marzari, F. Mauri, R. Mazzarello, S. Paolini, A. Pasquarello, L. Paulatto, C. Sbraccia, S. Scandolo, G. Sclauzero, A.P. Seitsonen, A. Smogunov, P. Umari, R.M. Wentzcovitch, QUANTUM ESPRESSO: a modular and open-source software project for quantum simulations

of materials, *J Phys Condens Matter*, 21 (2009) 395502.

[42] S. Baroni, S. de Gironcoli, A. Dal Corso, P. Giannozzi, Phonons and related crystal properties from density-functional perturbation theory, *Rev. Mod. Phys.*, 8, 73, 515 (2001).

[43] J.P. Perdew, A. Zunger, Self-interaction correction to density-functional approximations for many-electron systems, *Physical Review B*, 23 (1981) 5048-5079.

[44] C. Hartwigsen, S. Goedecker, J. Hutter, Relativistic separable dual-space gaussian pseudopotentials from h to rn, *Phys. Rev. B*, 58 (1998) 3641.

[45] A.P. Drozdov, M.I. Eremets, I.A. Troyan, Superconductivity above 100 K in PH3 at high pressures, *arxiv*, (2015) 06224.

[46] D.V. Semenok, J.N. Guo, D. Zhou, W.H. Chen, T. Helm, A.G. Kvashnin, A.V. Sadakov, O.A. Sobolevsky, V.M. Pudalov, V.V. Struzhkin, C.Y. Xi, X.L. Huang, I.A. Troyan, Evidence for Pseudogap Phase in Cerium Superhydrides: CeH10 and CeH9, *arXiv:2307.11742*, (2023).

[47] W. Chen, X. Huang, D.V. Semenok, S. Chen, D. Zhou, K. Zhang, A.R. Oganov, T. Cui, Enhancement of superconducting properties in the La-Ce-H system at moderate pressures, *Nat Commun*, 14 (2023) 2660.

[48] I. Troyan, D.V. Semenok, A.G. Ivanova, A.V. Sadakov, D. Zhou, A.G. Kvashnin, I.A. Kruglov, O.A. Sobolevskiy, M.V. Lyubutina, D.S. Perekalin, T. Helm, S.W. Tozer, M. Bykov, A.F. Goncharov, V.M. Pudalov, I.S. Lyubutin, Non-Fermi-Liquid Behavior of Superconducting SnH4, *arXiv:2303.06339*, (2023).

[49] E.A. Yuzbashyan, B.L. Altshuler, Breakdown of the Migdal-Eliashberg theory and a theory of lattice-fermionic superfluidity, *Physical Review B*, 106 (2022).

[50] Y. Zhou, J. Guo, S. Cai, J. Zhao, G. Gu, C. Lin, H. Yan, C. Huang, C. Yang, S. Long, Y. Gong, Y. Li, X. Li, Q. Wu, J. Hu, X. Zhou, T. Xiang, L. Sun, Quantum phase transition from superconducting to insulating-like state in a pressurized cuprate superconductor, *Nature Physics*, 18 (2022) 406-410.

[51] J.A. Woollam, R.B. Somoano, P. O'Connor, Positive Curvature of the Hc2-versus-TcBoundaries in Layered Superconductors, *Physical Review Letters*, 32 (1974) 712-714.

[52] N.R. Werthamer, E. Helfand, P.C. Hohenberg, Temperature and Purity Dependence of the Superconducting Critical Field, Hc2. III. Electron Spin and Spin-Orbit Effects, *Physical Review*, 147 (1966) 295-302.

[53] T. Baumgartner, M. Eisterer, H.W. Weber, R. Flükiger, C. Scheuerlein, L. Bottura, Effects of neutron irradiation on pinning force scaling in state-of-the-art Nb3Sn wires, *Superconductor Science and Technology*, 27 (2014).

[54] A.V. Sadakov, V.A. Vlasenko, I.A. Troyan, O.A. Sobolevskiy, D.V. Semenok, D. Zhou, V.M. Pudalov, Vortex Phase Dynamics in Yttrium Superhydride YH(6) at Megabar Pressures, *J Phys Chem Lett*, (2023) 6666-6671.

[55] D.V. Semenok, I.A. Troyan, A.G. Ivanova, A.G. Kvashnin, I.A. Kruglov, M. Hanfland, A.V. Sadakov, O.A. Sobolevskiy, K.S. Pervakov, I.S. Lyubutin, K.V. Glazyrin, N. Giordano, D.N. Karimov, A.L. Vasiliev, R. Akashi, V.M. Pudalov, A.R. Oganov, Superconductivity at 253 K in lanthanum–yttrium ternary hydrides, *Materials Today*, 48 (2021) 18-28.

[56] J. Guo, S. Chen, W. Chen, X. Huang, T. Cui, Advances in the Synthesis and Superconductivity of Lanthanide Polyhydrides Under High Pressure, *Frontiers in Electronic Materials*, 2 (2022).

[57] Z. Li, X. He, C. Zhang, K. Lu, B. Min, J. Zhang, S. Zhang, J. Zhao, L. Shi, Y. Peng, S. Feng, Z. Deng, J. Song, Q. Liu, X. Wang, R. Yu, L. Wang, Y. Li, J.D. Bass, V. Prakapenka, S. Chariton, H. Liu, C. Jin, Superconductivity above 70 K observed in lutetium polyhydrides, *Science China Physics, Mechanics & Astronomy*, 66 (2023).

[58] H. Song, Z. Zhang, T. Cui, C.J. Pickard, V.Z. Kresin, D. Duan, High Tc Superconductivity in Heavy Rare Earth Hydrides, *Chinese Physics Letters*, 38 (2021).

[59] D.V. Semenok, D. Zhou, A.G. Kvashnin, X. Huang, M. Galasso, I.A. Kruglov, A.G. Ivanova, A.G. Gavriluk, W. Chen, N.V. Tkachenko, A.I. Boldyrev, I. Troyan, A.R. Oganov, T. Cui, Novel Strongly Correlated Europium Superhydrides, *J Phys Chem Lett*, 12 (2021) 32-40.

[60] M. Pena-Alvarez, J. Binns, M. Martinez-Canales, B. Monserrat, G.J. Ackland, P. Dalladay-Simpson, R.T. Howie, C.J. Pickard, E. Gregoryanz, Synthesis of Weaire-Phelan Barium Polyhydride, *J Phys Chem Lett*, 12 (2021) 4910-4916.

[61] W. Chen, D.V. Semenok, I.A. Troyan, A.G. Ivanova, X. Huang, A.R. Oganov, T. Cui, Superconductivity and equation of state of lanthanum at megabar pressures, *Physical Review B*, 102 (2020).

[62] C. Ji, B. Li, W. Liu, J.S. Smith, A. Majumdar, W. Luo, R. Ahuja, J. Shu, J. Wang, S. Sinogeikin, Y. Meng, V.B. Prakapenka, E. Greenberg, R. Xu, X. Huang, W. Yang, G. Shen, W.L. Mao, H.K. Mao, Ultrahigh-pressure isostructural electronic transitions in hydrogen, *Nature*, 573 (2019) 558-562.

[63] D. Semenok, Computational design of new superconducting materials and their targeted experimental synthesis, Doctoral program in materials science and engineering thesis, Skoltech, (2022).

[64] P.B. Allen, R.C. Dynes, Transition temperature of strong-coupled superconductors reanalyzed, *Physical Review B*, 12 (1975) 905-922.

[65] E. G.M., Interactions between electrons and lattice vibrations in a normal metal, *Journal of Experimental and Theoretical Physics*, 34 (1960).

SUPPORTING INFORMATION

Stabilization of high-temperature superconducting A15 phase La_4H_{23} below 100 GPa

Jianning Guo,^{1,†} Grigoriy Shutov,^{4,5,6,†} SuChen,¹ Yulong Wang,¹ Di Zhou,³ Tian Cui^{1,2}, Xiaoli Huang^{1,*} and Dmitrii Semenok^{3,*}

¹*State Key Laboratory of Superhard Materials, College of Physics, Jilin University, Changchun 130012, China*

²*School of Physical Science and Technology, Ningbo University, Ningbo 315211, China*

³*Center for High Pressure Science and Technology Advanced Research (HPSTAR), Beijing*

⁴ *Moscow Institute of Physics and Technology, 9 Institutsky Lane, Dolgoprudny 141700, Russia*

⁵ *Dukhov Research Institute of Automatics (VNIIA), Moscow 127055, Russia*

⁶ *Skolkovo Institute of Science and Technology, Skolkovo Innovation Center, 3 Nobel Street, Moscow 143026, Russia*

[†]These authors contributed equally to this work

*Corresponding authors, Email: huangxiaoli@jlu.edu.cn (X. Huang)
dmitrii.semenok@hpstar.ac.cn (D. Semenok)

Content

| | |
|---|----|
| 1. Thermodynamic calculations | S2 |
| 2. Electron, phonon, elastic and superconducting properties of La_4H_{23} | S7 |

1. Thermodynamic calculations

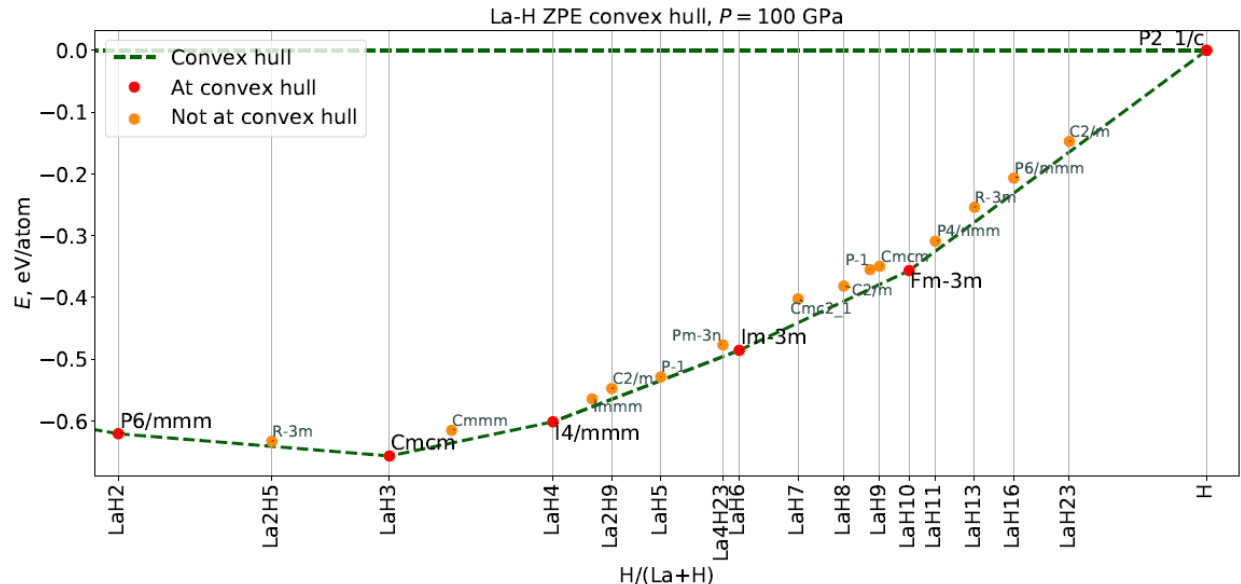


Figure S1. Convex hull of the La-H system calculated at 100 GPa and 0 K in harmonic approximation. Only those phases that lie less than 30 meV/atom from the convex hull are shown. Zero-point energy (ZPE) was included in the calculations.

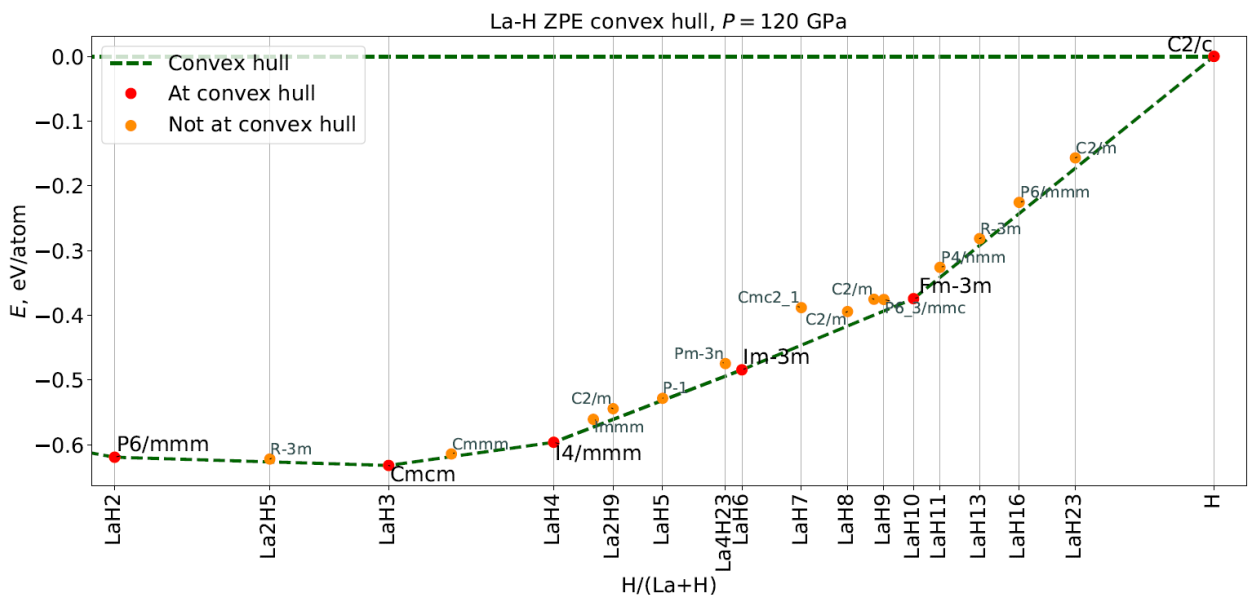


Figure S2. Convex hull of the La-H system calculated at 120 GPa and 0 K in harmonic approximation. Only those phases that lie less than 30 meV/atom from the convex hull are shown. Zero-point energy (ZPE) was included in the calculations.

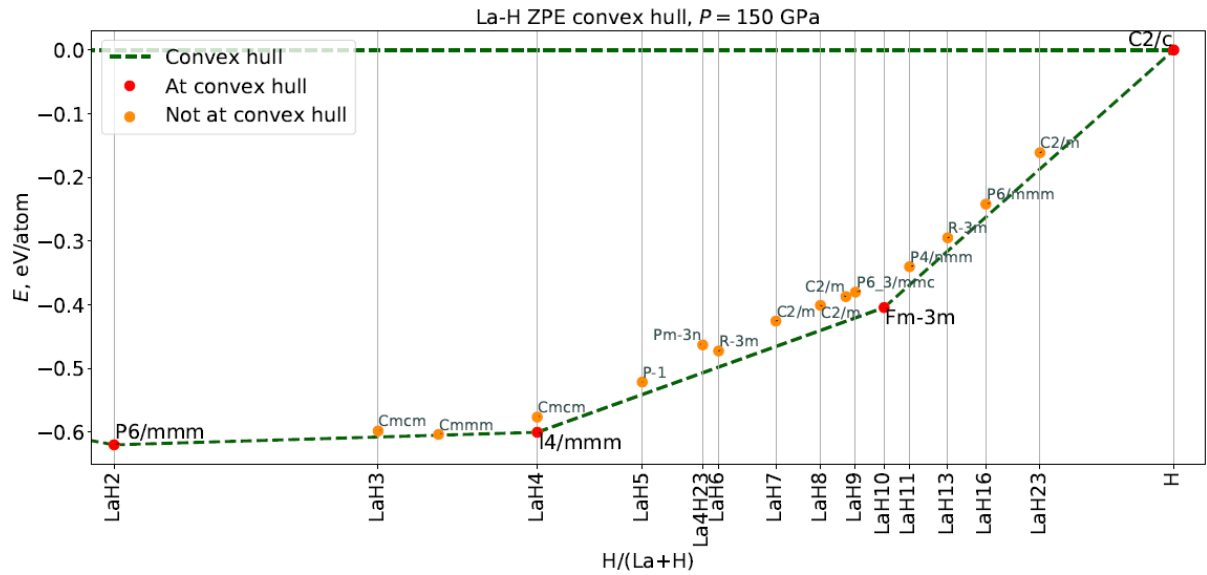


Figure S3. Convex hull of the La-H system calculated at 150 GPa and 0 K in harmonic approximation. Only those phases that lie less than 30 meV/atom from the convex hull are shown. Zero-point energy (ZPE) was included in the calculations.

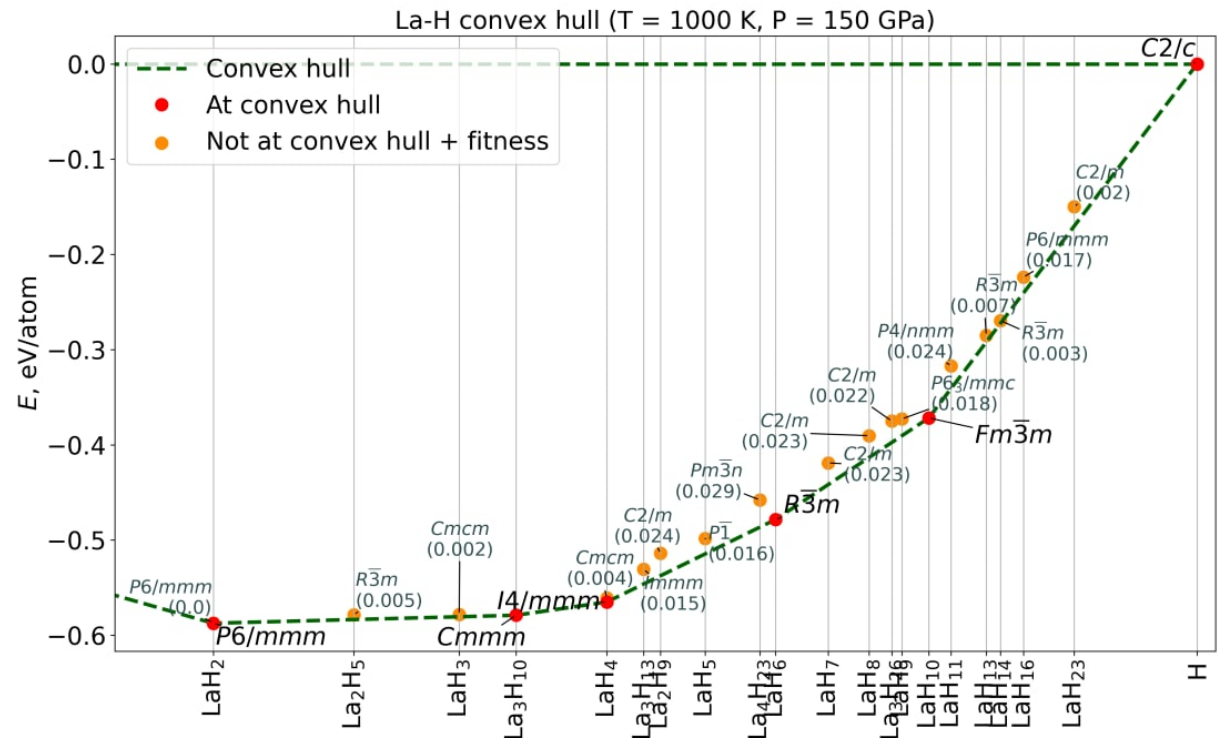


Figure S4. Convex hull of the La-H system calculated at 150 GPa and 1000 K in harmonic approximation. Only those phases that lie less than 30 meV/atom from the convex hull are shown. Zero-point energy (ZPE) was included in the calculations. The numbers in parentheses correspond to the distance of the connections from the convex hull in eV/atom.

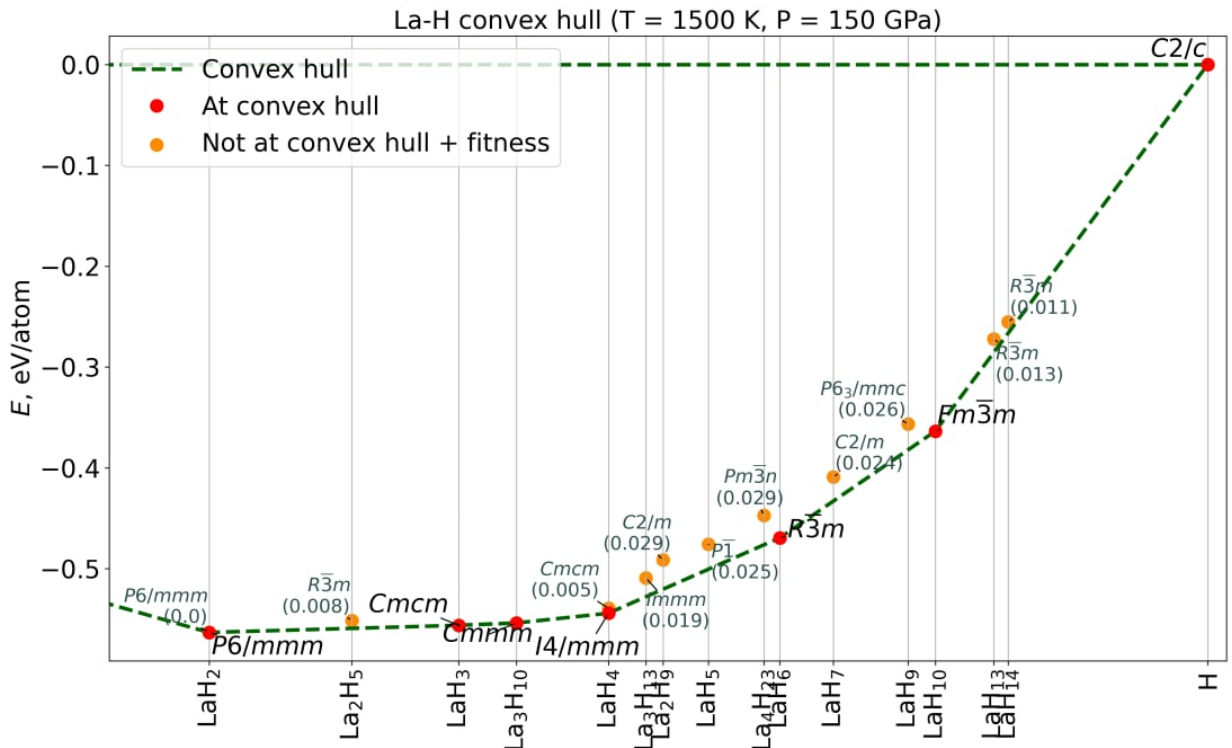


Figure S5. Convex hull of the La-H system calculated at 150 GPa and 1500 K in harmonic approximation. Only those phases that lie less than 30 meV/atom from the convex hull are shown. Zero-point energy (ZPE) was included in the calculations. The numbers in parentheses correspond to the distance of the connections from the convex hull in eV/atom.

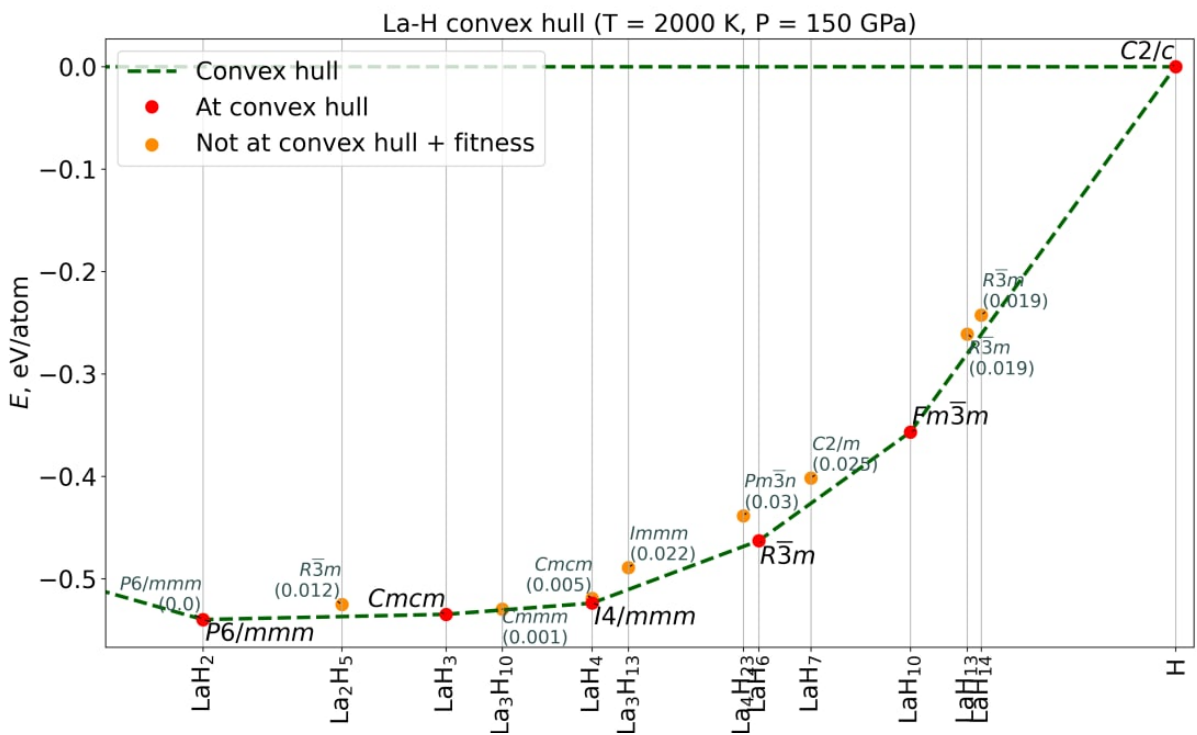


Figure S6. Convex hull of the La-H system calculated at 150 GPa and 2000 K in harmonic approximation. Only those phases that lie less than 30 meV/atom from the convex hull are shown. Zero-point energy (ZPE) was included in the calculations. The numbers in parentheses correspond to the distance of the connections from the convex hull in eV/atom.

Table S1. Enthalpies of formation of various lanthanum hydrides (in eV/atom) at 100 GPa and 0 K (Figure S1). ZPE stands for the zero-point energy. X, Y are coordinates of lanthanum hydrides on the two-dimensional convex hull diagram. Fitness is the distance from the convex hull line.

| Space Group | Formula | X | E | ZPE | E+ZPE | Y | ZPE Y | Old fitness | ZPE fitness |
|---------------|---------------------------------|---------|----------|---------|----------|----------|----------|-------------|-------------|
| <i>Fm-3m</i> | LaH ₁₀ | 0,90900 | -0,62980 | 0,15270 | -0,47710 | -0,26900 | -0,35680 | 0,03340 | 0,00 |
| <i>C2/m</i> | La ₂ H ₉ | 0,81800 | -0,04020 | 0,19930 | 0,15910 | -0,52800 | -0,54790 | 0,01110 | 0,01730 |
| <i>P4/nmm</i> | LaH ₁₁ | 0,91700 | -0,72460 | 0,22610 | -0,49850 | -0,29300 | -0,30920 | 0,00 | 0,01620 |
| <i>C2/m</i> | LaH ₂₃ | 0,95800 | -0,96460 | 0,24850 | -0,71610 | -0,14400 | -0,14760 | 0,00280 | 0,01710 |
| <i>R-3m</i> | LaH ₁₃ | 0,92900 | -0,77100 | 0,21920 | -0,55180 | -0,22830 | -0,25420 | 0,02910 | 0,02420 |
| <i>C2/m</i> | LaH ₈ | 0,88900 | -0,52480 | 0,20630 | -0,31840 | -0,35250 | -0,38190 | 0,01520 | 0,02460 |
| <i>P-1</i> | La ₃ H ₂₆ | 0,89700 | -0,57270 | 0,21120 | -0,36150 | -0,32890 | -0,35530 | 0,01810 | 0,03130 |
| <i>Cmcm</i> | LaH ₉ | 0,90 | -0,60650 | 0,21910 | -0,38730 | -0,33050 | -0,34970 | 0,01110 | 0,02950 |
| <i>P6/mmm</i> | LaH ₁₆ | 0,94100 | -0,83340 | 0,21400 | -0,61940 | -0,17310 | -0,20700 | 0,03810 | 0,02430 |
| <i>Pm-3n</i> | La ₄ H ₂₃ | 0,85200 | -0,26240 | 0,18580 | -0,07660 | -0,43590 | -0,47710 | 0,02510 | 0,01910 |
| <i>Cmcm</i> | LaH ₃ | 0,75 | 0,47480 | 0,19560 | 0,67040 | -0,64960 | -0,65710 | 0,00 | 0,00 |
| <i>R-3m</i> | La ₂ H ₅ | 0,71400 | 0,83010 | 0,18910 | 1,01920 | -0,62760 | -0,63330 | 0,00210 | 0,00820 |
| <i>I4/mmm</i> | LaH ₄ | 0,80 | 0,08260 | 0,18800 | 0,27060 | -0,57490 | -0,60180 | 0,00 | 0,00 |
| <i>P6/mmm</i> | LaH ₂ | 0,66700 | 1,29180 | 0,17300 | 1,46480 | -0,61050 | -0,62110 | 0,00 | 0,00 |
| <i>Fm-3m</i> | La | 0,00 | 8,12600 | 0,02700 | 8,15290 | 0,00 | 0,00 | 0,00 | 0,00 |
| <i>Cmc2_1</i> | LaH ₇ | 0,87500 | -0,44290 | 0,23010 | -0,21290 | -0,40030 | -0,40270 | 0,20 | 0,03860 |
| <i>Imm</i> | La ₃ H ₁₃ | 0,81200 | -0,00250 | 0,19660 | 0,19410 | -0,54340 | -0,56460 | 0,00670 | 0,01280 |
| <i>P2_1/c</i> | H | 1,00 | -1,20950 | 0,26180 | -0,94770 | 0,00 | 0,00 | 0,00 | 0,00 |
| <i>Im-3m</i> | LaH ₆ | 0,85700 | -0,30910 | 0,17550 | -0,13360 | -0,43320 | -0,48600 | 0,01630 | 0,00 |
| <i>Cmmm</i> | La ₃ H ₁₀ | 0,76900 | 0,34050 | 0,19630 | 0,53690 | -0,60430 | -0,61560 | 0,01310 | 0,02050 |
| <i>P-1</i> | LaH ₅ | 0,83300 | -0,15900 | 0,19900 | 0,04 | -0,50540 | -0,52910 | 0,00 | 0,00570 |

Table S2. Enthalpies of formation of various lanthanum hydrides (in eV/atom) at 120 GPa and 0 K (Figure S2). ZPE stands for the zero-point energy. X, Y are coordinates of lanthanum hydrides on the two-dimensional convex hull diagram. Fitness is the distance from the convex hull line.

| Space Group | Formula | X | E | ZPE | E+ZPE | Y | ZPE Y | Old fitness | ZPE fitness |
|-----------------|---------------------------------|---------|----------|---------|----------|----------|----------|-------------|-------------|
| <i>Fm-3m</i> | LaH ₁₀ | 0,90900 | -0,22280 | 0,16470 | -0,05800 | -0,29430 | -0,37440 | 0,02550 | 0,00 |
| <i>C2/m</i> | La ₂ H ₉ | 0,81800 | 0,54580 | 0,20900 | 0,75480 | -0,53020 | -0,54440 | 0,01120 | 0,01650 |
| <i>C2/m</i> | La ₃ H ₂₆ | 0,89700 | -0,13350 | 0,21010 | 0,07660 | -0,34360 | -0,37530 | 0,02230 | 0,02450 |
| <i>P4/nmm</i> | LaH ₁₁ | 0,91700 | -0,32380 | 0,23210 | -0,09160 | -0,31160 | -0,32600 | 0,00 | 0,01550 |
| <i>C2/m</i> | LaH ₂₃ | 0,95800 | -0,62820 | 0,25530 | -0,37290 | -0,15580 | -0,15680 | 0,80 | 0,01600 |
| <i>P6_3/mmc</i> | LaH ₉ | 0,90 | -0,16390 | 0,20280 | 0,03900 | -0,33590 | -0,37560 | 0,01610 | 0,01780 |
| <i>C2/m</i> | LaH ₈ | 0,88900 | -0,07070 | 0,21110 | 0,14050 | -0,36550 | -0,39430 | 0,01600 | 0,02240 |
| <i>Imm</i> | La ₃ H ₁₃ | 0,81200 | 0,59440 | 0,20540 | 0,79980 | -0,54440 | -0,56080 | 0,00730 | 0,01190 |
| <i>R-3m</i> | LaH ₁₃ | 0,92900 | -0,39150 | 0,21570 | -0,17580 | -0,24790 | -0,28150 | 0,02240 | 0,01060 |
| <i>Pm-3n</i> | La ₄ H ₂₃ | 0,85200 | 0,26420 | 0,19630 | 0,46050 | -0,43980 | -0,47470 | 0,02830 | 0,01940 |
| <i>Cmcm</i> | LaH ₃ | 0,75 | 1,20050 | 0,20370 | 1,40430 | -0,62870 | -0,63210 | 0,00 | 0,00 |
| <i>R-3m</i> | La ₂ H ₅ | 0,71400 | 1,60400 | 0,19630 | 1,80030 | -0,61980 | -0,62220 | 0,00210 | 0,00440 |
| <i>I4/mmm</i> | LaH ₄ | 0,80 | 0,70150 | 0,19800 | 0,89950 | -0,57540 | -0,59630 | 0,00 | 0,00 |
| <i>P6/mmm</i> | LaH ₂ | 0,66700 | 2,13760 | 0,18030 | 2,31790 | -0,61240 | -0,61940 | 0,00 | 0,00 |
| <i>Fm-3m</i> | La | 0,00 | 10,11560 | 0,02970 | 10,14530 | 0,00 | 0,00 | 0,00 | 0,00 |
| <i>P6/mmm</i> | LaH ₁₆ | 0,94100 | -0,47160 | 0,21550 | -0,25620 | -0,18870 | -0,22560 | 0,02920 | 0,01710 |
| <i>Cmc2_1</i> | LaH ₇ | 0,87500 | 0,06060 | 0,23610 | 0,29670 | -0,38760 | -0,38820 | 0,02420 | 0,05810 |
| <i>Im-3m</i> | LaH ₆ | 0,85700 | 0,20360 | 0,19 | 0,39360 | -0,44190 | -0,48430 | 0,01430 | 0,00 |
| <i>Cmmm</i> | La ₃ H ₁₀ | 0,76900 | 1,01130 | 0,20290 | 1,21420 | -0,60550 | -0,61430 | 0,00120 | 0,00420 |
| <i>P-1</i> | LaH ₅ | 0,83300 | 0,39880 | 0,20830 | 0,60710 | -0,50980 | -0,52830 | 0,00 | 0,00320 |
| <i>C2/c</i> | H | 1,00 | -0,93280 | 0,26620 | -0,66660 | 0,00 | 0,00 | 0,00 | 0,00 |

Table S3. Enthalpies of formation of various lanthanum hydrides (in eV/atom) at 150 GPa and 0 K (Figure S3). ZPE stands for the zero-point energy. X, Y are coordinates of lanthanum hydrides on the two-dimensional convex hull diagram. Fitness is the distance from the convex hull line.

| Space Group | Formula | X | E | ZPE | E+ZPE | Y | ZPE Y | Old fitness | ZPE fitness |
|-------------|---------------------------------|---------|----------|---------|----------|----------|----------|-------------|-------------|
| P-1 | LaH ₅ | 0,83300 | 1,18930 | 0,21930 | 1,40860 | -0,50900 | -0,52140 | 0,00 | 0,01960 |
| C2/c | H | 1,00 | -0,55310 | 0,27 | -0,28300 | 0,00 | 0,00 | 0,00 | 0,00 |
| Fm-3m | LaH ₁₀ | 0,90900 | 0,35600 | 0,16370 | 0,51970 | -0,31900 | -0,40440 | 0,01730 | 0,00 |
| Cmcm | LaH ₄ | 0,80 | 1,57860 | 0,21760 | 1,79620 | -0,57 | -0,57640 | 0,00450 | 0,02390 |
| Cmcm | LaH ₃ | 0,75 | 2,22530 | 0,21300 | 2,43830 | -0,59870 | -0,59820 | 0,00530 | 0,00950 |
| I4/mmm | LaH ₄ | 0,80 | 1,57510 | 0,19720 | 1,77230 | -0,57350 | -0,60030 | 0,00 | 0,00 |
| P6/mmm | LaH ₂ | 0,66700 | 3,33740 | 0,18570 | 3,52300 | -0,61230 | -0,62 | 0,00 | 0,00 |
| Fm-3m | La | 0,00 | 12,95520 | 0,04 | 12,99510 | 0,00 | 0,00 | 0,00 | 0,00 |
| C2/m | La ₃ H ₂₆ | 0,89700 | 0,48300 | 0,22040 | 0,70340 | -0,36140 | -0,38720 | 0,01800 | 0,03880 |
| R-3m | LaH ₁₃ | 0,92900 | 0,14100 | 0,22960 | 0,37050 | -0,27080 | -0,29490 | 0,01490 | 0,02060 |
| P4/nmm | LaH ₁₁ | 0,91700 | 0,24290 | 0,24020 | 0,48320 | -0,32970 | -0,34030 | 0,00 | 0,02850 |
| Pm-3n | La ₄ H ₂₃ | 0,85200 | 1,01160 | 0,20940 | 1,22100 | -0,43650 | -0,46310 | 0,03480 | 0,04370 |
| C2/m | LaH ₂₃ | 0,95800 | -0,15650 | 0,26540 | 0,10900 | -0,16620 | -0,16120 | 0,40 | 0,02540 |
| P6 3/mmc | LaH ₉ | 0,90 | 0,45140 | 0,21310 | 0,66460 | -0,34630 | -0,38020 | 0,02290 | 0,04040 |
| C2/m | LaH ₈ | 0,88900 | 0,56940 | 0,22200 | 0,79140 | -0,37850 | -0,40090 | 0,01360 | 0,03940 |
| P6/mmm | LaH ₁₆ | 0,94100 | 0,02690 | 0,22920 | 0,25610 | -0,21460 | -0,24200 | 0,01910 | 0,02020 |
| C2/m | LaH ₇ | 0,87500 | 0,74220 | 0,20890 | 0,95110 | -0,39330 | -0,42560 | 0,02710 | 0,03990 |
| R-3m | LaH ₆ | 0,85700 | 0,92860 | 0,21260 | 1,14120 | -0,44810 | -0,47260 | 0,01130 | 0,02530 |
| Cmmm | La ₃ H ₁₀ | 0,76900 | 1,96300 | 0,21470 | 2,17760 | -0,60130 | -0,60350 | 0,00 | 0,00140 |

2. Electron, phonon, elastic and superconducting properties of La_4H_{23}

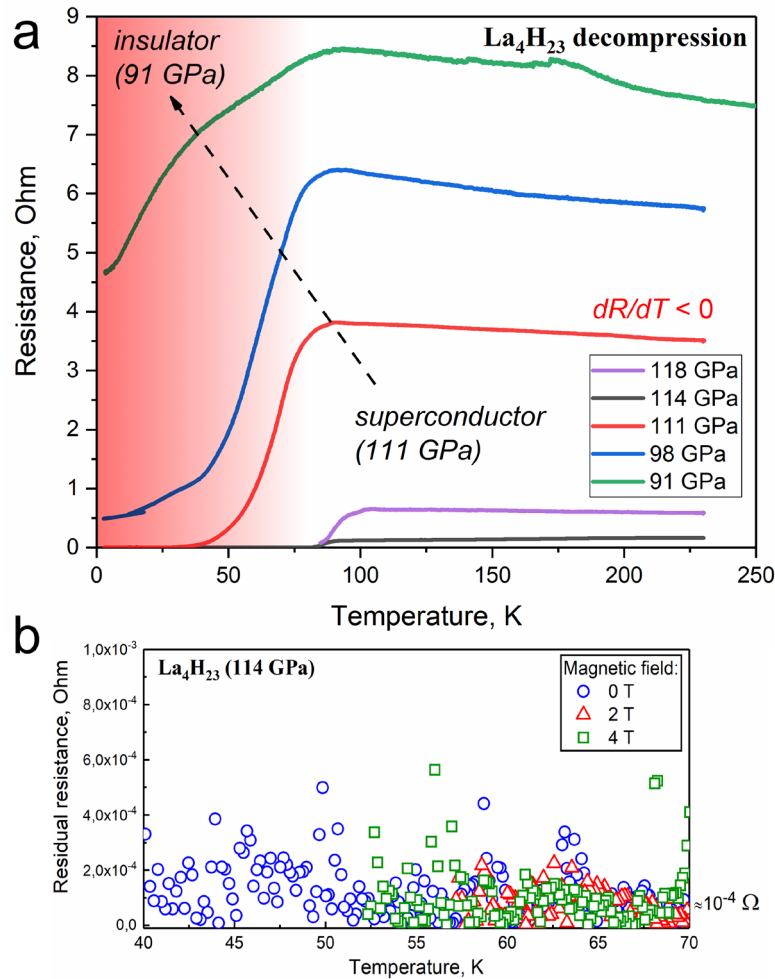


Figure S7. Experimental transport properties of La_4H_{23} . (a) Decompression of the DAC H1 and temperature dependence of the electrical resistivity of the sample in real scale. Pronounced increase in electrical resistance in 10-100 times at $T > T_c$ is observed during decompression due to the beginning of the metal-insulator transition. The anomaly at 114 GPa is an exception. (b) Residual resistance of the sample detected in the superconducting state in magnetic fields of 0-4 T.

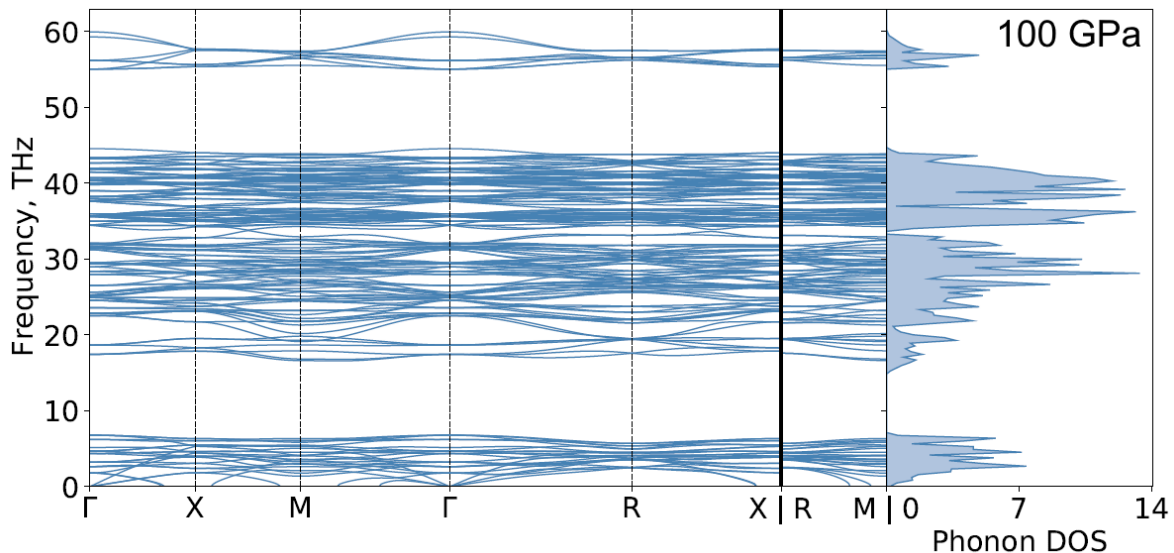


Figure S8. Phonon band structure and corresponding density of states of La_4H_{23} at 100 GPa in harmonic approximation. The compound has a small number of imaginary phonon modes, which are likely to disappear when anharmonic effects are considered.

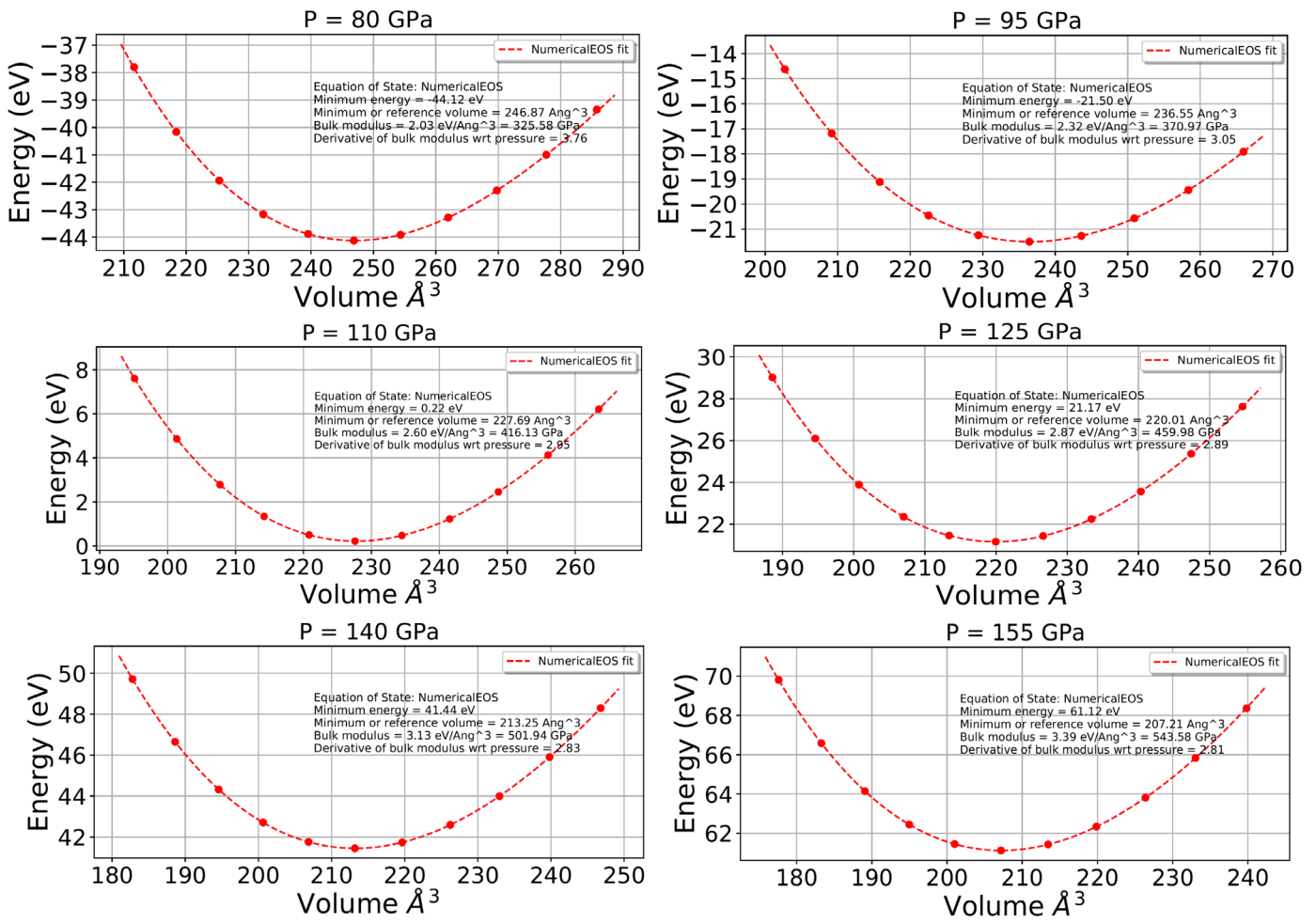


Figure S9. Equation of state, bulk modulus (B) and its derivative (dB/dP) of La_4H_{23} at pressures from 80 to 155 GPa. Calculations were done using VASP code with the PAW PBE pseudopotentials for La and H.

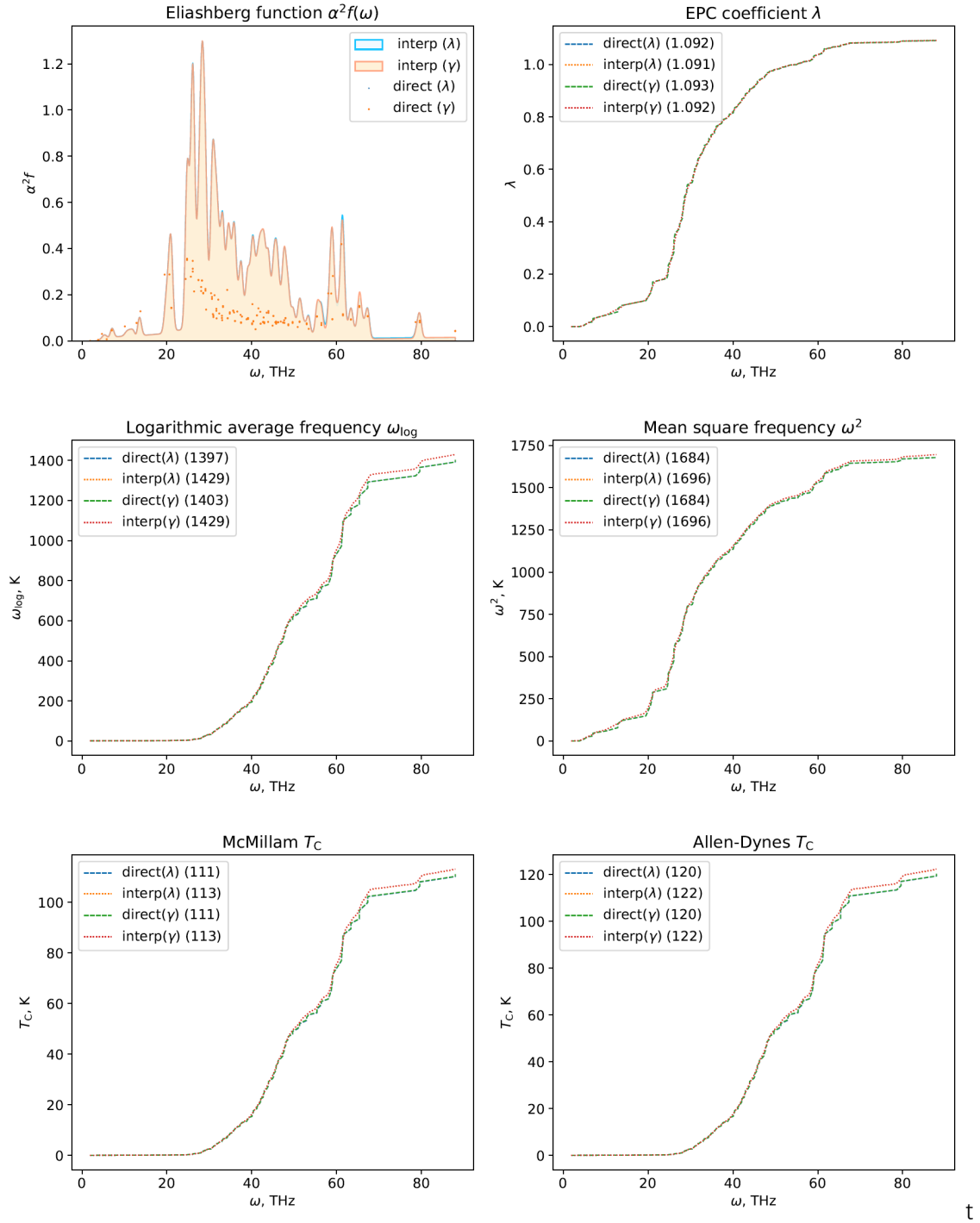


Figure S10. Superconducting state parameters and Eliashberg function for La₄H₂₃ at 150 GPa calculated using PBE HGH pseudopotentials for La and H atoms, q -mesh was $2 \times 2 \times 2$.